ORIGINAL ARTICLE

Spherical NiWO₄-reduced graphene oxide nanocomposite for effective visible light driven photocatalytic activity for the decolourisation of organic pollutants

Sathish Mohan Botsa [a,*], **M. Jagadeesh Babu** [b,*], **P. Suresh** [c], **P. Kalyani** [d], **B. Venkateswararao** [e], **R. Muralikrishna** [a]

[a] National Centre for Polar and Ocean Research, Ministry of Earth Sciences, Vasco Da Gama, Goa 403804, India
[b] Dept. of Physcial, Nuclear Chemistry and Chemical Oceanography, Andhra University, Visakhapatnam 530003, India
[c] Dept. of Chemistry, JNTU Kakinada, Andhra Pradesh 533003, India
[d] Dept. of Microbiology, Andhra University, Visakhapatnam 530003, India
[e] Dept. of Engineering Chemistry, Andhra University, Visakhapatnam 530003, India

Abstract A hybrid nanocomposite of nickel tungstate – reduced graphene oxide (NiWO₄-RGO) was prepared using a surfactant free hydrothermal approach. Resulting hybrid nanocomposite powder was grounded for forty minutes to ensure homogeneity and avoid agglomerations of particles. Resulting nanocomposite was characterised by XRD, FTIR, FESEM and EDX analysis. Photocatalytic activities of the characterised catalyst were examined by the decolourisation of Methylene blue (MB) and *ortho*-nitrophenol (ONP) under visible light irradiation were conducted at room temperature. The results confirmed that 15 wt% NiWO₄-RGO composite was degraded almost completely MB (95%) and ONP (82%) within 150 and 240 min respectively under visible light sources. The catalyst was reused and stable for successive six runs with loss of 10% of degradation rate.

© 2020 Published by Elsevier B.V. on behalf of King Saud University. This is an open access article under the CC BY-NC-ND license (http://creativecommons.org/licenses/by-nc-nd/4.0/).

* Corresponding authors.
E-mail address: bsathish401@gmail.com (S.M. Botsa).

1. Introduction

During few decades, human beings are facing huge challenges in energy calamity and environmental preservation. Due to the use of water combined with different types of dyes as the

promising material in various industries, the pollution is getting more environmental problems mainly effect the aquatic life (Chala et al., 2014). Therefore, scientists are admiring to the contraption of new sustainable energy storage methods, among which electrochemical splitting of water with the help of semiconductor photocatalyst is the promising method to remove toxic pollutants from industrial effluents as the degradation method could mineralise organic pollutants completely to CO_2, H_2O and less and/or non toxic compounds without generating any secondary pollutions. In addition, the operating process does not require high energy consumption (Chatterjee and Dasgupt, 2005). In recent years, vast research has been carried out to explore the novel properties of metal oxide semiconductors, mostly advantageous in solar cells, photovoltaic devices Sunlight-driven photocatalysts such as TiO_2 (Thiruvenkatachari, 2008), doped TiO_2 (Moradi et al., 2018), Cu_2O (Muthukumaran and Gnanamoorthy, 2020), Fe_2O_3 (Sivaranjani et al., 2019), ZnO (Chen et al., 2017), SnO_2 (Prakash et al., 2016) etc. are extensively used. After that, instead of metal oxide photocatalyst, mixed metal oxide nano semiconductors $BiFeO_3$ (Mushtaq et al., 2018), $LaFeO_3$ (Hu et al., 2012), $SrTiO_3$ (Konstas et al., 2018), $BiVO_4$ (Zhou et al., 2011), $Fe_2Mo_3O_4$ (Suresh et al., 2014), $Bi_2Mo_3O_4$ (Changsheng et al., 2013), $CuWO_4$ (Jagadeesh Babu et al., 2020), Bi_2WO_6 (Deepthi et al., 2018), $ZnWO_4$ (Zhang et al., 2010), $CuBi_2O_4$ (Paliki et al., 2018) etc. are used as a photocatalyst.

Tungstates has received great attention by researchers due to their wide range applications in sensing applications for Hg, humidity and photocatalyst, photoelectrochemical because of their unique properties (Jagadeesh Babu et al., 2020; Eranjaneya et al., 2019). They reported that $NiWO_4$ were successfully synthesized by decomposition approach, hydrothermal method (Hosseini et al., 2018), electrochemical method (Pourmortazavi et al., 2018), and molten salts route (AlShehri et al., 2017). Hydrothermal route has attracted more interest towards the preparation of various nanomaterials or composites due to the ability of this route to form good, large crystal phase. However, $NiWO_4$ has broad bandgap which struggles to export the electrons and resulting in less photocatalytic activity (Jagadeesh Babu et al., 2020).

Presently, there has been more delight in fabricating and utilizing novel graphene oxide (GO) containing metal tungstate nanocomposites for environmental remediation by the degradation or elimination of hazardous organic contaminants and heavy metals (Botsa and Basavaiah, 2019; Nair Abhinav and Jagadeesh Babu, 2017) Among the utilized nanomaterials in water treatment, GO having a honeycomb-like structure with its interesting 2D carbon framework, has more fascinate interest from the few decade for its unique specific surface area, high charge carrier mobility and electron conductivity (Sree et al., 2020; Mohan et al., 2018). We have deliberated the competence of the $NiWO_4$-RGO composite as induced visible light active photocatalyst for the decolourisation of Methylene blue and Ortho nitrophenol organic pollutants. A probable photocatalytic degradation mechanism is proposed and the superlative photocatalytic efficacy is ascribed to the electron–hole pair separation was achieved by the combination of RGO with $NiWO_4$.

2. Experimental details

2.1. Materials

Nickel nitrate ($Ni(NO_3)_2 \cdot 6H_2O$), sodium tungstate dihydrate ($Na_2WO_4 \cdot 2H_2O$) were purchased from Sigma Aldrich and Merck Co., were used without further purification for analysis. The selected dye stuffs were collected from Himedia Lab, India and Doubled distilled water from local supplier for the making solution.

2.2. Graphene oxide preparation

Graphene Oxide (GO) was synthesized from graphite powder according to the modified hummers method reported by Hummers and Offeman (Hummers and Offeman, 1958). In brief, 1.0 g of graphite powder and 0.5 g of $NaNO_3$ were added into 23 ml of cooled concentrated H_2SO_4. Then, gradually added 3 g of $KMnO_4$ with continuous stirring followed by cooling and temperature of the reaction mixture was maintained below 10 °C using an ice bath. Later, the ice bath was removed and the reaction mixture was further stirred for 30 min at 35 °C. The distilled water (46 ml) was added slowly to increase in temperature to 100 °C and it continues further 15 min. The reaction was terminated by the addition of distilled water (140 ml) followed by 30% H_2O_2 (10 ml) aqueous solution. The resultant solid yield was detached by centrifugation and washed repeatedly with 5% HCl solution until sulphate anion could not be detected with $BaCl_2$. The resultant solid GO was dried in vacuum at 50 °C.

2.3. NiWO₄-RGO composite preparation

For the preparation of $NiWO_4$, the equimolar ratio of Ni $(NO_3)_2$ and Na_2WO_4 solutions were prepared with 50 ml milli Q water separately followed by stirring for 30 min to homogeneous nature. In addition five times higher concentration of NaOH solution was added to the $Ni(NO_3)_2$ solution and stirred for almost 30 min. Meanwhile, to above mixture suspension, Na_2WO_4 solution was added slowly drop wise and the blend was transferred into a Teflon-lined stainless-steel autoclave with sealed and employed in hot air stabilizer at heating of 170 °C for 18 h. After, the autoclave was cooled to get room temperature and the obtained product was centrifuged, washed with Milli Q water and ethanol successively. Utmost, the yield was dried in an oven during overnight to get the purest form of $NiWO_4$. We have employed the same procedure for synthesizing the NWR composites by stoichiometry with GO loading to the $NiWO_4$ to form 5%, 10% and 15% $NiWO_4$-RGO composites. The advantage of this synthesis is the materials prepared without using any reducing agents like $NaBH_4$, $LiAlH_4$ and so on.

$$Ni(NO_3)_2 \ + \ 2 \ NaOH \ \rightarrow \ Ni(OH)_2 \ + \ Na(NO_3)_2 \qquad (1)$$

$$Ni(OH)_2 \ + \ Na_2WO_4 \ \rightarrow \ NiWO_4 \ + \ 2NaOH \qquad (2)$$

$$Ni(NO_3)_2 \ + \ Na_2WO_4 \ + \ GO \ \rightarrow \ NiWO_4\text{-}RGO \qquad (3)$$

2.4. Characterisation

In order to study the properties of prepared NiWO4-RGO composite were characterized by various characterization techniques. Initially, X-ray powder diffraction (XRD) pattern of
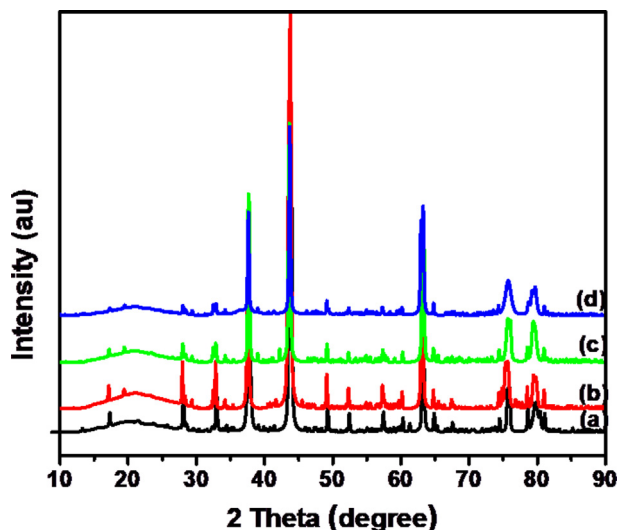
Fig. 1 XRD patterns of hydrothermally prepared (a) NiWO4 (b) NiWO4-RGO (5%) (c) NiWO4-RGO (10%) and (d) NiWO4-RGO (15%) composites.

as-prepared nanoparticles samples were taken by a Bruker D8 Advance X-ray diffractometer with Cu-Kα radiation (1.5406 Å, X-ray tube voltage = 35 kV and current = 35 m A) with the scan range of 2θ from 0° to 90°. FESEM images of NiWO4-RGO samples were taken using the instrument FEI (Model-Nova Nano SEM 450) operating at 15 kV and the EDX was used to analyse the chemical composition of as prepared sample using BRUKER EDS detector (Model-XFlash 6/10). Fourier transform infrared spectrum of the NiWO4/RGO samples was recorded by FTIR spectrophotometer (IR prestige 21, Shimadzu) in the range 4000–400 cm^{-1}, spectral output was recorded by transmittance as a function of wave number.

2.5. Photocatalytic activity

Photocatalytic efficiency of characterized NiWO4-RGO was evaluated by the degradation of Methylene Blue (MB) and *ortho*-nitrophenol (O-NP) in the light irradiation, 400 W metal halide lamp as a light source for irradiation. UV radiation below 350 nm is eliminated by surrounding the sample with a water jacket. 100 mg of the photocatalyst powder was added into 100 ml of the model dye pollutant solution and the suspension mixture was magnetically stirred for 30 min in a dark room to ensure adsorption-desorption thermal equilibrium between photocatalyst surface and dye molecule. The suspension mixture was further exposed to light emanating and 5 ml aliquots were pipette out at regular time intervals. 0.45 μm Millipore filters were utilized for filtration to separate the
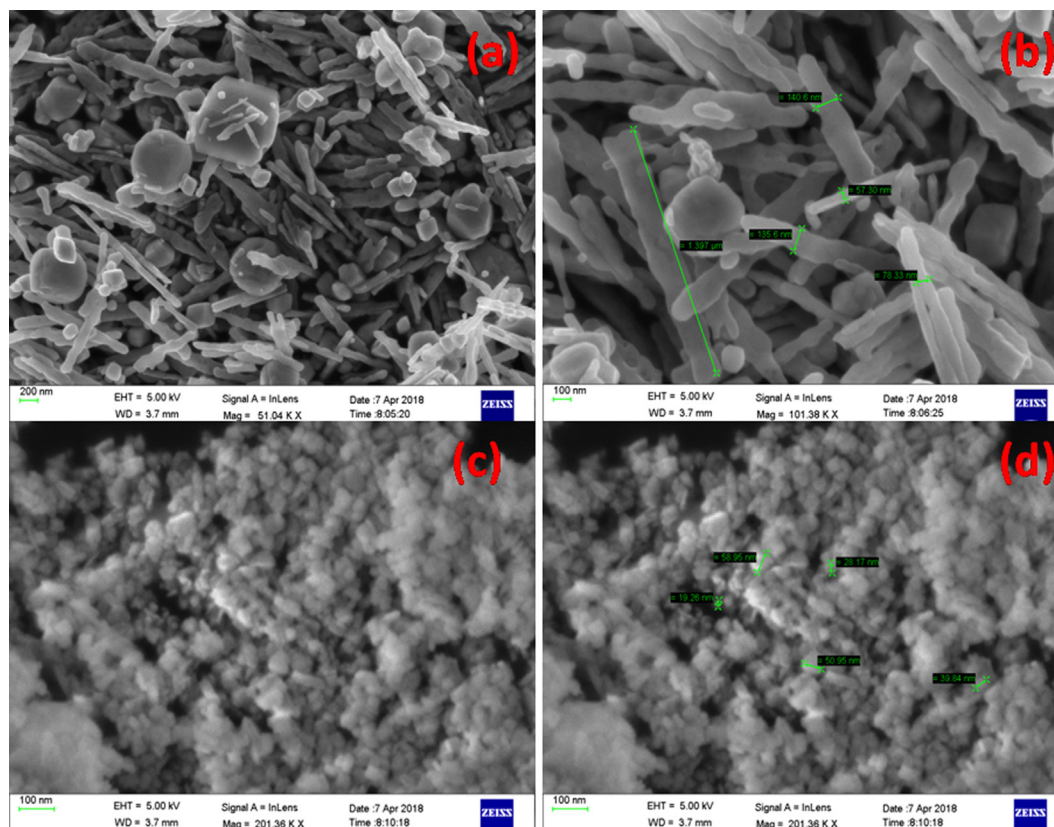
Fig. 2 SEM images of pure NiWO4 (a-b) and 15 wt% of RGO loaded NiWO4 (c-d).

suspended catalyst. The progress of decolourisation of tested pollutant was examined by using UV–Visible absorption spectrum. Degradation rate of dye is calculated by the following equation (4).

$$\% \text{ degradation of dye } = [(C_0 - Ct)/C_0] \times 100 \qquad (4)$$

Where, C_0 and C_t are respectively initial and final volumes of absorbance of the dye.

3. Results and discussion

Fig. 1 depicts X-ray diffraction (XRD) Patterns of NiWO$_4$ and Graphene oxide loaded – NiWO$_4$ at various wt% i.e. 5%, 10% and 15% were synthesized by surfactant free hydrothermal method. From the Fig. 1, we can say that all peaks could be indexed to NiWO$_4$ was confirmed with JCPDS card NO 15-0755. Absence of extra peaks or impurity peaks indicates that the sample obtained in phase pure. The strong peak was appeared at 10.6° confirmed the GO was produced. All diffraction peaks of NiWO$_4$-RGO composites are presented as the NiWO$_4$. The pure single crystalline phase was formed without other relevant peaks as the hydrothermal method is facile, easy to operate and enhance the crystal growth and purity of

compound. The average crystalline sizes (S) of hydrothermally prepared composites were measured using Debey-Scherrer's equation (5).

$$S = K\lambda/\beta\cos\theta \qquad (5)$$

Where λ is the wavelength, θ is the angle of diffraction, β is the full width at half maximum and Scherrer's constant is K usually taken as 0.94. The size of NiWO$_4$ was found to be 34 nm and NiWO$_4$-RGO (15%) composite shown lesser size 19.3 nm. Due to change in size of prepared composite, the surface area may be changes (Jagadeesh Babu et al., 2020). In general, smaller size particles having greater surface area which leads to enhanced photocatalytic activity.

In order to get the information regarding surface morphology of synthesized nanocomposites, field emission scanning electron microscopy (FESEM) has been employed. Fig. 2 depicts the FESEM images of NiWO$_4$ and 15 wt% of NiWO$_4$-RGO composite at different magnifications. Although, the small variation in GO loading amount to obtained desirable composites they possess agglomeration due to overlay of tungstates on RGO layer and exhibited nanomicrospherical shape comprised of uniform sheets with their structure was greatly developed. From the Fig. 2a, it can be seen that pure NiWO$_4$
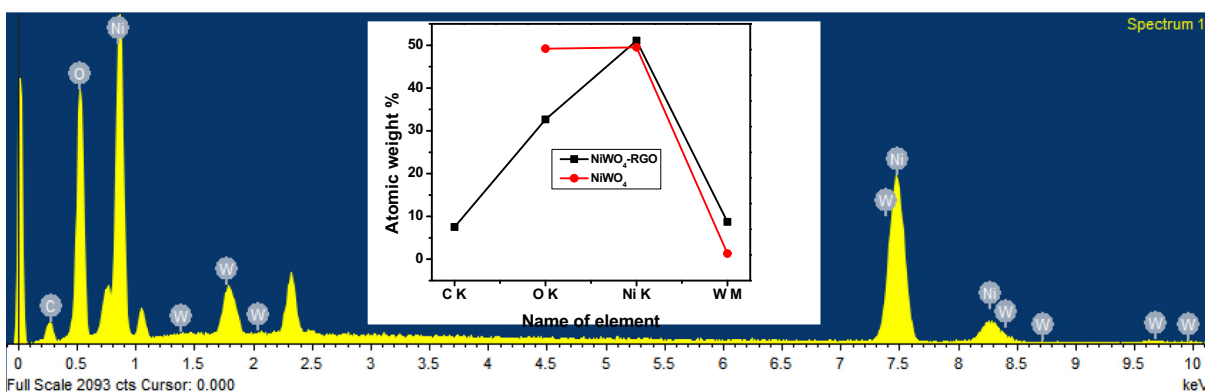
Fig. 3   Energy Dispersive X-ray Analysis of pure NiWO$_4$ (a) and NiWO$_4$-RGO 15% (b).
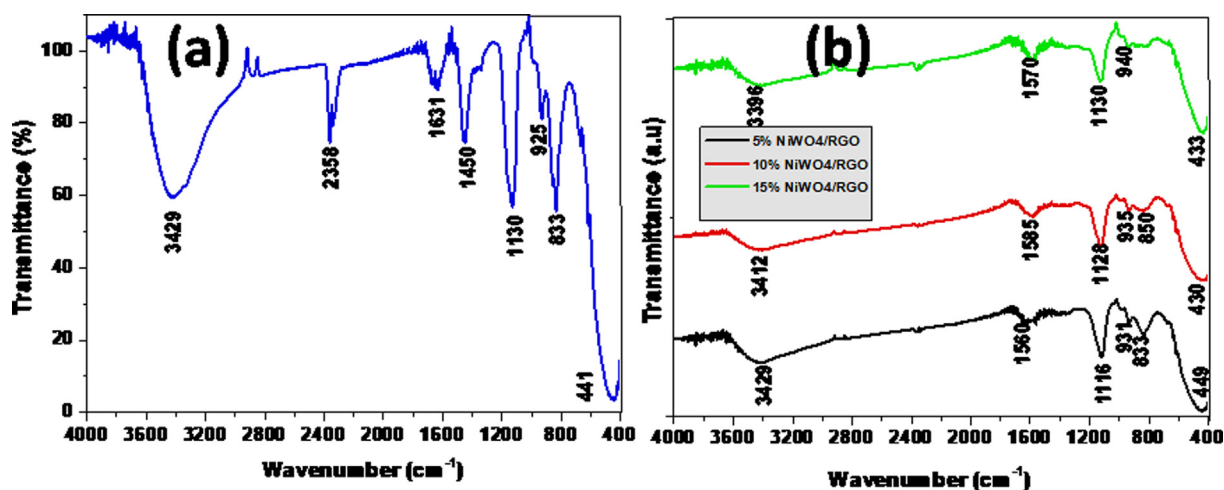
Fig. 4   FTIR spectra of (a) NiWO$_4$ and (b) NiWO$_4$-RGO composites.
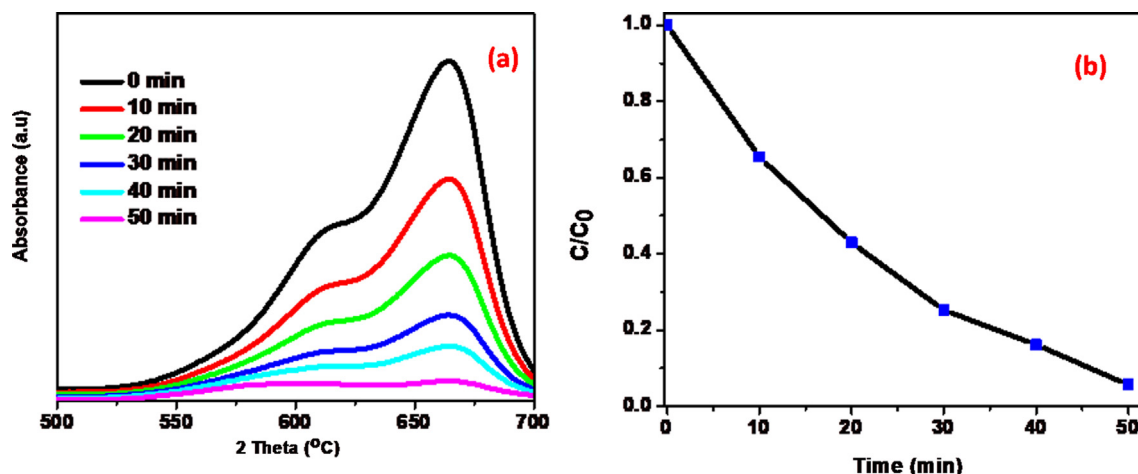
Fig. 5 (a) Absorbance spectra of MB in presence of 15 wt% NiWO$_4$-RGO nanocomposite. (b) Plot of C/C$_0$ as a function of irradiation time.

consists of relatively uniform and smooth surface plate like/rod like microstructures with average length of 1.397 μm and diameter 140.6 nm combined with spherical nanoparticles. Whereas RGO loaded NiWO$_4$ nanoparticles are changing their shapes to spherical structure with porous nature, due to agglomeration of NPs as shown in Fig. 2b. Some kind of uniformity can be seen in the structure of prepared composites.

The energy dispersive X-ray analysis of hydrothermally synthesised NiWO$_4$ and NiWO$_4$-RGO nanocomposite were carried out is depicted in Fig. 3, in which the characteristic peaks corresponding to Ni (nickel), W (tungsten), C (carbon) and O (oxygen) are seen and there is no traces of precursors which can be concluded that the final products through hydrothermal method were obtained in pure form.

Fig. 4 reveals that FTIR spectra for fabricated tungstates within the range 4000–400 cm^{-1}. From Fig. 4a and 4b, we can conclude that the absorption bands at 3390–3429 cm^{-1} and 1560–1630 cm^{-1} indicates the existence of ─OH stretching and bending vibrations related to water molecule absorption. The weak absorption bands appeared within the absorption range at 835–850 cm^{-1} can be evidenced to the stretching mode of W─O bonds in the joints with WO$_4$ tetrahedral. The bands nearly observed at 930 cm^{-1} related to the stretching mode of the W═O bond (Mancheva et al., 2007). In Fig. 4b spectra exhibits the peaks nearly at 1160 cm^{-1} and 1550 cm^{-1} corresponding to the stretching frequencies of C─O─H and C═C respectively, which suggests that the GO has been effectively reduced during the process (Ossonon

Table 1 MB dye degradation using various tungstate based composites.

S. No	Catalyst Name	Catalyst dose (g)	Dye Conc. (ppm)	Light source (lamp)	Degradation rate (%)	Time (min)	Ref. No
1	NiWO$_4$-ZnO-NRGO	0.02	10	250 W Hg	99.3	120	(Sadiq et al., 2017)
2	CaWO$_4$	0.025	10	sunlight	98	180	(Farsi and Barzgari, 2015)
3	CuWO$_4$-GO	0.05	10	Metal Halide	100	60	(Medidi et al., 2018)
4	CoWO$_4$	1	10	Hg lamp	40	120	(Montinia et al., 2010)
	CuWO$_4$				70	120	
	ZnWO$_4$				95	120	
5	Bi$_2$WO$_6$	2 × 2 cm^3	20	500 W halogen	86	100	(Rajendran et al., 2018)
	CdS				72	100	
	PVA assisted Bi$_2$WO$_6$-CdS				92	100	
6	BaWO$_4$-GO	0.05	10	400 W metal halide	100	90	(Sunitha et al., 2017)
7	Bi$_2$WO$_6$-GO	0.05	10	500 W Xe	88.1	120	(Zhou and Zhu, 2012)
8	WO$_3$/CdWO$_4$	0.1	10	500 W xenon	95	50	(Aslam et al., 2015)
9	SrWO$_4$		1.15 × 10^{-5}	54 W Philips	72	390	(Dirany et al., 2020)
10	Pr$_2$(WO$_4$)$_3$	0.1	25	Hg	99.7	60	(Pourmortazavi and Nasrabadi, 2017)
11	NiWO$_4$	50	10	Heber multi-lamp	100	50	(Saravanakumar et al., 2019)
12	NiWO$_4$-RGO	0.05	10	400 W metal halide	98.5	50	Present study
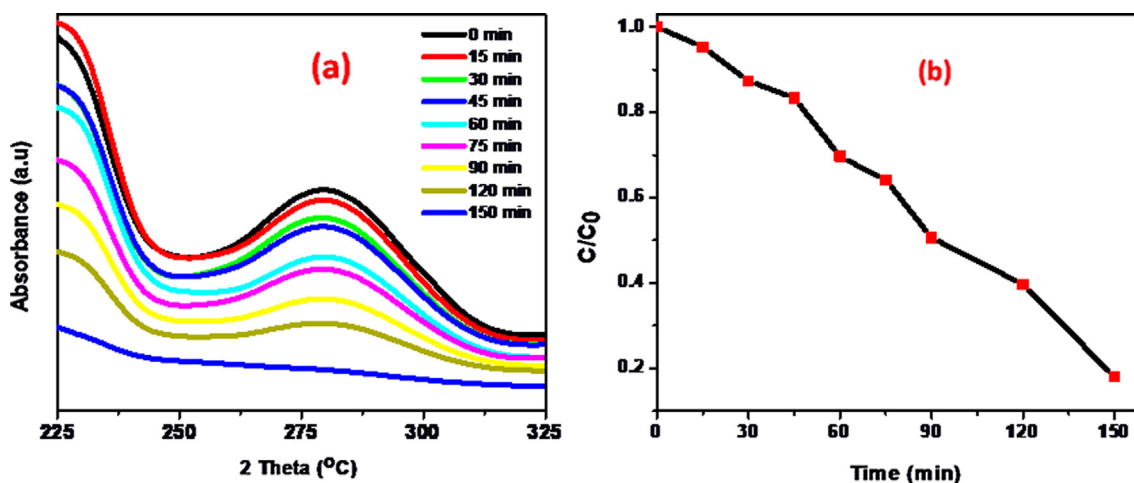
Fig. 6 (a) Absorbance spectra of O-NP in presence of 15 wt% NiWO$_4$-RGO nanocomposite and (b) Plot of C/C$_0$ as a function of irradiation time.

and B'elanger, 2017). All of results further confirmed that the synthesized crystalline materials are tungstate composites.

3.1. Photocatalytic performance

Discoloration of MB and O-NP were taken as model reactions to determine the photocatalytic efficiency of as synthesised tungstates. Temporal variations of spectral changes during photodegradation of MB as a function of irradiation time are shown in Fig. 5a. As expected, the NiWO$_4$ was initially tested on MB dye solution, but it doesn't show any significant degradation rate (31%). Remarkable degradation rate was noticed using the RGO based NiWO$_4$ composites were studied on same dye at the conditions of 100 mg catalyst quantity and 100 ml of 10 mg/L dye solution at pH-10. RGO has assembled

with metal tungstate found to be an excellent in photocatalytic efficiency for the decolourisation of dyes (Upadhyay et al., 2014) and found to be 63% degradation of MB dye using NiWO$_4$-RGO (5%) (Fig S1 in ESI). The effect of RGO loading on activity of composites were studied and optimized threshold mass percent of RGO to attain greater photocatalytic performance (Sree et al., 2020). This leads to increase the GO dose in synthesis of NiWO$_4$-RGO composite and their photocatalytic performance was mostly depends on the interface between NiWO$_4$ and RGO which facilitates the charge separation of photo-electrons and photo-holes, finally decrease the recombination rate and 10% GO loaded NiWO$_4$ composite exhibits better degradation percentage (81%) and NiWO$_4$-RGO (15%) was the most effective for photocatalytic degradation of MB dye using stimulation of visible light
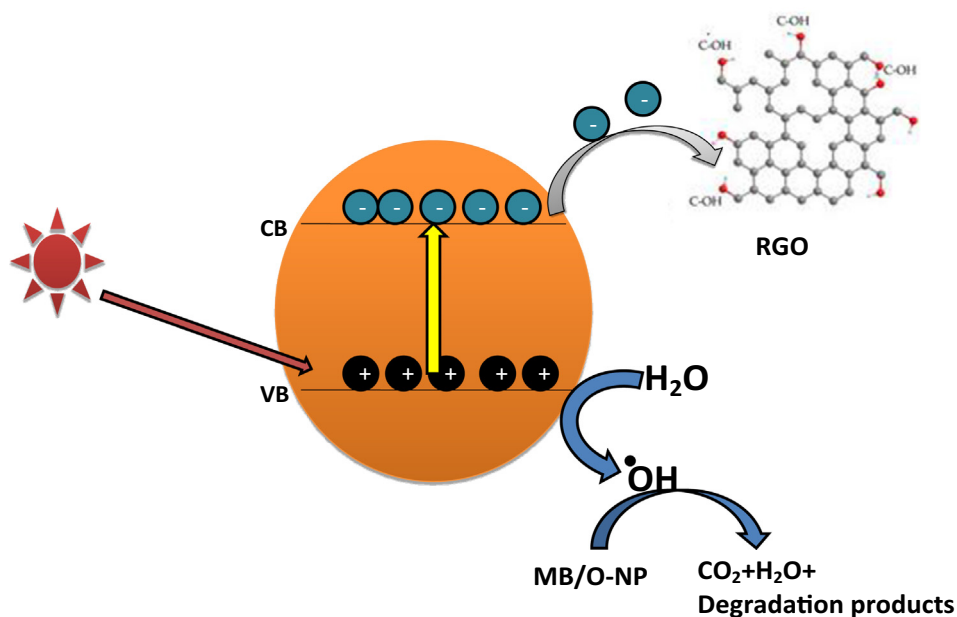
Fig. 7 Schematic representation of MB/O-NP degradation mechanism using NiWO$_4$-RGO Nanocomposite.
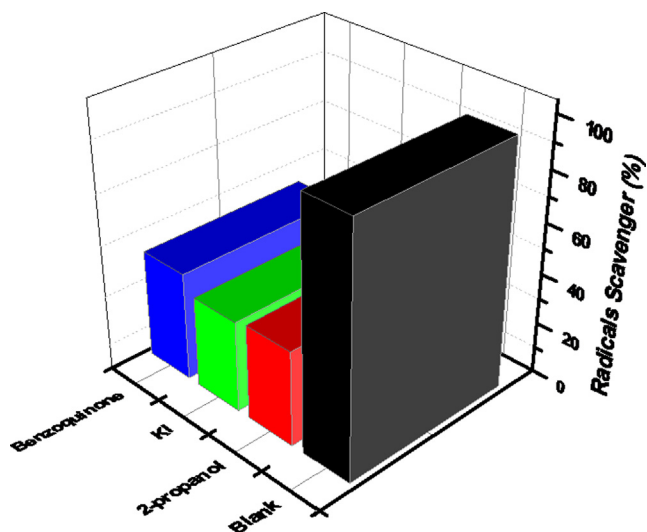
Fig. 8 ROS analysis of photodegradation of dye by prepared tungstate composites.

(95%). The π-π stacking is formed between aromatic rings of RGO and dye pollutant assists the adsorption of dye pollutants on to the surface of catalyst hence increasing the quenching of dyes.

From the Fig. 5a, it can be seen that as increasing visible light exposure on MB aqueous solution contains synthesised NiWO₄-RGO nanocomposite decrease in absorption at 665 nm clearly signifies that the chromophoric structure of MB was decomposed completely almost and the hypochromic shift was attributed. Fig. 5b indicates the plots of C/C_0 vs exposure of time for the MB aqueous solution. Based on the spectral data, it can be concluded that 95% of 10 ppm MB dye was degraded in presence of 100 mg of 15 wt% RGO loaded NiWO₄ photocatalyst under visible light irradiation.

Significantly, the hydrothermal assisted synthesis of NiWO₄-RGO composite exhibited better photocatalytic activity towards the MB degradation than similar class of tungstates which reported earlier as shown in table 1.
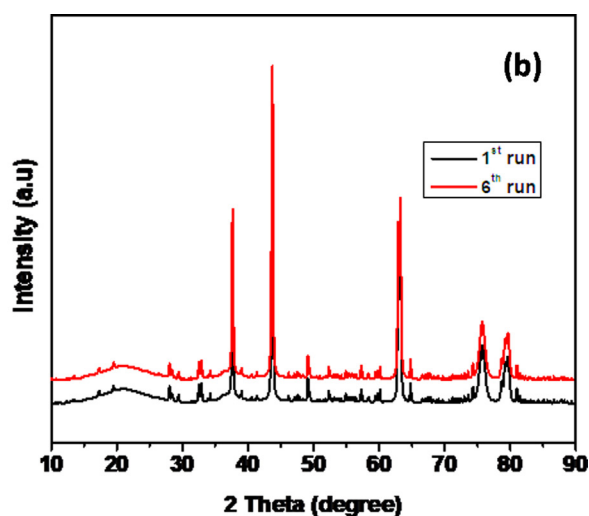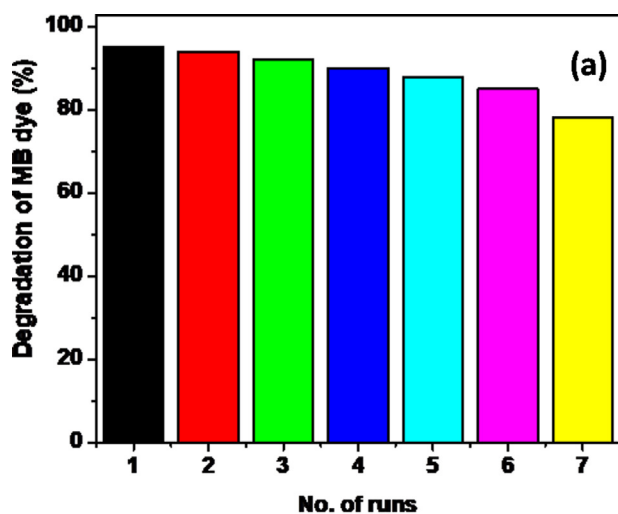
Based on this experiment, further studies were conducted on photocatalytic degradation of O-NP aqueous solution using 15 wt% NiWO₄-RGO composite. Fig. 6a depicts the temporal variation of spectral changes of 100 ml of 10 ppm O-NP solution with 100 mg of NiWO₄-RGO nanocomposite. From the Fig. 6a, decrease in absorbance of O-NP as a function of exposure time in under 400 W metal halide lamp as visible light source. Fig. 6b indicates that the plots of C/C_0 vs exposure of time for the O-NP solution. Based on the spectral data, it can be concluded that 82% of 10 ppm O-NP was degraded in presence of 100 mg of 15 wt% RGO loaded NiWO₄ photocatalyst under visible light irradiation.

The rate constants for degradation of MB and O-NP under visible light irradiation were examined with the help of the following equation (6).

$$ln(C/C_0) = -k_{obs}t \qquad (6)$$

From the linear plot of ln(C/Co) with irradiation time, the observed degradation rates (k) of MB and O-NP in presence of hydrothermally synthesised hybrid nanocomposite were determined to be 1.06×10^{-6} and 1.66×10^{-5} min^{-1}, respectively.

Suggested photocatalytic degradation mechanism of MB and O-NP is given as follows: startlingly, the semiconductor materials (NiWO₄-RGO) absorb the energy in the form of photons in presence of visible light irradiation. Electrons are ejected from valance band to conduction band, resulting electron-hole pairs are generated at the photocatalyst surface. Then, photoinduced electrons are transferred from the nanocomposite to the RGO, which could efficiently reduce the electron and holes recombination. Afterwards, the high oxidation potential of the holes is more responsible to degradation of MB and O-NP by the oxidation of pollutants. Schematic representation of MB/O-NP degradation mechanism is shown in Fig. 7.

3.2. Reactive oxygen species assay

In context to photocatalytic degradation mechanism, identification of the reactive oxygen species ROS) such as h$^+$, ·OH and ·O$_2^-$ is most important. Hence, such ROS species were identified by using 2-propanol, KI and Benzoquinone for the

Fig. 9 Reusability (a) and sustainability (b) of prepared photocatalyst NiWO₄-RGO (15%).

confirmation of ˙OH, holes and ˙O_2^- radicals. The tested dye molecule reacts with these ROS species and finally produced deminerialized products like H_2O and CO_2 (Botsa and Basavaiah, 2020). Remarkable removal rate (97.1%) was recorded in absence of scavenger and the photodegradation rate is very less when tested with scavenger (Fig. 8). Hence, NiWO$_4$-RGO (15%) composite possess greater photocatalytic efficacy due to create more active sites on their surface which can accommodate more dye molecules, this may be presence of RGO in composite.

3.3. Reusability and sustainability

The photocatalyst was examined under reusability after photocatalytic process. For that, the catalyst was washed properly and used it in next degradation process. The NiWO$_4$-RGO composite was re-run for six runs continuously and found to be loss of 10% degradation rate (Fig. 9a). In addition, the stability was checked by XRD patterns after six cycles, there is no apparent change in its phase (Fig. 9b).

4. Conclusion

NiWO$_4$ and the NiWO$_4$-RGO nanocomposite with different wt% of RGO have been synthesised via hydrothermal method. These materials are characterised by XRD, FESEM, EDX and FTIR. Characterisation study revealed that as synthesised nanocomposite was phase pure, plate like and spherical microstructures with porous nature. These materials degrade MB and O-NP very effectively under visible light irradiation. Photo catalytic degradation of 100 ml aqueous solutions of MB and O-NP (10 mg/L) containing 100 mg of the dispersed catalyst occurred 94% and 82% in 150 and 240 min respectively. The catalyst was reused and stable for successive six runs with loss of 10% of degradation rate.

Declaration of Competing Interest

The authors declare that they have no known competing financial interests or personal relationships that could have appeared to influence the work reported in this paper.

Acknowledgement

Appendix A. Supplementary data

Supplementary data to this article can be found online at https://doi.org/10.1016/j.arabjc.2020.09.017.

References

Chala, S., Wetchakun, K., Phanichphant, S., Inceesungvorn, B., Wetchakun, N., 2014. Enhanced visible-light-response photocatalytic degradation of methylene blue on Fe-loaded BiVO$_4$ photocatalyst. J. Alloys Comp. 597, 129–135.

Chatterjee, D., Dasgupt, S., 2005. Visible light induced photocatalytic degradation of organic pollutants. J. Photochem. Photobiol. 6 (2–3), 186–205.

Thiruvenkatachari, R., 2008. Saravanamuthu Vigneswaran & Il Shik Moon, A review on UV/TiO2 photocatalytic oxidation process. Korean J. Chem. Eng. 25, 64–72.

Moradi, V., Jun, M.B.G., Blackburn, A., Herring, R.A., 2018. Significant improvement in visible light photocatalytic activity of Fe doped TiO$_2$ using an acid treatment process. Appl. Surf. Sci. 427, 791–799.

Muthukumaran, M., Gnanamoorthy, G., Varun Prasath, P., Abinaya, M., Dhinagaran, G., Sagadevan, Suresh, Mohammad, Faruq, Chun Oh, Won, Venkatachalam, K., 2020. Enhanced photocatalytic activity of Cuprous Oxide nanoparticles formalachite green degradation under the visible light radiation. Mater. Res. Express. 7, 015038.

Sivaranjani, R., Thayumanavan, A., Sriram, S., 2019. Photocatalytic activity of Zn-doped Fe$_2$O$_3$ nanoparticles:a combined experimental and theoretical study. Bull. Mater. Sci. 42, 185.

Chen, X., Zhansheng, W.u., Liu, D., Gao, Z., 2017. Preparation of ZnO photocatalyst for the efficient and rapid photocatalytic degradation of Azo dyes. Nanoscale Res. Lett. 12, 143.

Prakash, K., Senthil Kumar, P., Pandiaraj, S., Saravanakumar, K., Karuthapandian, S., 2016. Controllable synthesis of SnO$_2$ photocatalyst with superior photocatalytic activity for the degradation of methylene blue dye solution. J. Exp. Nanosci. 11 (14), 1138–1155.

Mushtaq, F., Chen, X., Hoop, M., Torlakcik, H., Pellicer, E., Sort, J., Gattinoni, C., Nelson, B.J., Pané, S., 2018. Piezoelectrically enhanced photocatalysis with BiFeO$_3$ nanostructures for efficient water remediation. Iscience 4, 236–246.

Hu, R., Ch, L., Sun, Y., Jia, H., Su, H., 2012. Photocatalytic activities of LaFeO$_3$ and La$_2$FeTiO$_6$ in p – chlorophenol degradation under visible light. Catal. Commun. 29, 35–39.

Konstas, P.S., Konstantinou, I., Petrakis, D., Albanis, T., 2018. Development of SrTiO$_3$ photocatalysts with visible light response using amino acids as dopant sources for the degradation of organic pollutants in aqueous systems. Catalysts 8, 528.

Zhou, B., Zhao, X., Liu, H., Qu, J., Huang, C.P., 2011. Synthesis of visible-light sensitive MBiVO4 (M = Ag, Co and Ni) for the photocatalytic degradation of organic pollutants. Seperat. Purif. Technol. 77, 275–282.

Suresh, P., Rajesh, B., Rao, T.S., Rao, A.V.P., 2014. Rapid photo catalytic degradation of crystal violet and carmine indigo under sun light by Fe$_2$Mo$_3$O$_{12}$. J. Appl. Chem. 3 (4), 1670–1678.

Changsheng, G., Jian, X., Shanfeng, W., Yuan, Z., Yan, H., 2013. Photodegradation of sulfamethazine in an aqueous solution by a bismuth molybdate photocatalyst. Catal. Sci. Technol. 3, 1603–1611.

Jagadeesh Babu, M., Botsa, S.M., Jhansi Rani, S., Venkateswararao, B., Muralikrishna, R., 2020. Enhanced photocatalytic degradation of cationic dyes under visible light irradiation by CuWO$_4$-RGO nanocomposite. Adv. Compos. Hybrid Mater. 3, 205–212.

Deepthi, K., Suresh, P., Umabala, A.M., Rao, A.V.P., 2018. Visible light assisted photocatalytic degradation of Methyl orange and Congo red using Bi$_2$WO$_6$ prepared by solid-state metathesis. Asian J. Chem. 30, 998–1002.

Zhang, L., Xu, T., Zhao, X., Zhu, Y., 2010. Controllabla synthesis of Bi$_2$MoO$_6$ and effect of morphology and variation in local structure on photocatalytic activities. Appl. Catal. B 98, 138–146.

Paliki, A.K., Botsa, S.M., Sailaja, B.B.V., 2018. Catalytic activity of graphene oxide hybridized ZnWO4 for dyes degradation and oxidation of functionalized benzyl alcohols. MOJ Biorg. Org. Chem. 2 (5), 230–234.

Eranjaneya, H., Adarakatti, P.S., Siddaramanna, A., 2019. Nickel tungstate nanoparticles: synthesis, characterization and electrochemical sensing of mercury (II) ions. J. Mater. Sci.: Mater. Electron. 30, 3574–3584.

Hosseini, S., Farsi, H., Moghiminia, S., Zubkov, T., Lightcap, I.V., Rile, A., Peters, D.G., Li, Z., 2018. Nickel tungstate (NiWO₄) nanoparticles/graphene composites: preparation and photoelectrochemical applications. Semicond. Sci. Technol. 33, 5.

Pourmortazavi, S.M., Nasrabadi, M.R., Karimi, M.S., Mirsadeghi, S., 2018. Evaluation of photocatalytic and supercapacitor potential of nickel tungstate nanoparticles synthesized by electrochemical method. New J. Chem. 42, 19934–19944.

AlShehri, S.M., Ahmed, J., Alzahrania, A.M., Ahamada, T., 2017. Synthesis, characterization, and enhanced photocatalytic properties of NiWO4 nanobricks. New J. Chem. 41, 8178–8186.

Botsa, S.M., Basavaiah, K., 2019. Removal of Nitrophenols from wastewater by monoclinic CuO/RGO nanocomposite. Nanotechnol. Environ. Eng. 4 (1), 1.

Nair Abhinav, K., Jagadeesh Babu, P., 2017. TiO₂ nanosheetgraphene oxide based photocatalytic hierarchical membrane for water purification. Surf. Coating. Technol. 320, 259–262.

Sree, G.S., Botsa, S.M., Reddy, B.J.M., Ranjitha, K.V.B., 2020. Enhanced UV-Visible triggered photocatalytic degradation of Brilliant green by Reduced Graphene Oxide based NiO and CuO ternary nanocomposite and their antimicrobial activity. Arab. J. Chem. 13 (4), 5137–5150.

Mohan, B.S., Ravi, K., Anjaneyulu, R.B., Sree, G.S., Basavaiah, K., 2018. Fe₂O₃/RGO nanocomposite photocatalyst: Effective degradation of 4-Nitrophenol. Physica B 553, 190–194.

Hummers Jr., W.S., Offeman, Richard E., 1958. Preparation of Graphitic oxide. J. Am. Chem. Soc. 80 (6), 1339.

Mancheva, M.N., Iordanova, R.S., Klissurski, D.G., Tyuliev, G.T., Kunev, B.N., 2007. Direct mechanochemical synthesis of nanocrystalline NiWO₄. J. Phys. Chem. C. 111 (3), 1101–1104.

Ossonon, Benjamin Diby, B'elanger, Daniel, 2017. Synthesis and characterization of sulfophenylfunctionalized reduced graphene oxide sheets. RSC Adv. 7, 27224.

Upadhyay, R.K., Soin, N., Roy, S.S., 2014. Role of graphene/metal oxide composites as photocatalysts, adsorbents and disinfectants in water treatment: a review. RSC Adv. 4, 3823.

Sadiq, M.M.J., Shenoy, U.S., Bhat, D.K., 2017. NiWO₄-ZnO-NRGO ternary nanocomposite as an efficient photocatalyst for degradation of methylene blue and reduction of 4-nitrophenol. J. Phys. Chem. Solids 109, 124–133.

Farsi, Hossein, Barzgari, Zahra, Askari, Seyede Zahra, 2015. Sunlight-induced photocatalytic activity of nanostructured calcium tungstate for methylene blue degradation. Res. Chem. Intermed. 41, 5463–5474.

Medidi, S., Markapurapu, S., Kotupalli, M.R., Chinnam, R.K.R., Susarla, V.M., Gandham, H.B., Sanasi, P.D., 2018. Visible light photocatalytic degradation of methylene blue and malachite green dyes with CuWO₄-GO nanocomposite. Modern Res. Cataly. 7, 2.

Montinia, T., Gombaca, V., Hameeda, A., Felisarid, L., Adamia, G., Fornasiero, P., 2010. Synthesis, characterization and photocatalytic performance of transitionmetal tungstates. Chem. Phys. Lett. 498, 113–119.

Rajendran, R., Varadharajan, K., Jayaraman, V., Singaram, B., Jeyaram, J., 2018. Photocatalytic degradation of metronidazole and methylene blue by PVA-assisted Bi₂WO₆–CdS nanocomposite film under visible light irradiation. Appl. Nanosci. 8, 61–78.

Sunitha, M., Soma Sekhar, R., Ravali, B., Reddy, C.R.K., Mahalakshmi, S.V., Sruthi, V., Douglas, S.P., 2017. Visible light photocatalytic degradation of methylene blue and malachite green dyes with BaWO₄-GO nanocomposite. Int. J. Environ., Agric. Biotechnol. 2 (3), 1173–1183.

Zhou, F., Zhu, Y., 2012. Significant photocatalytic enhancement in methylene blue degradation of Bi₂WO₆ photocatalysts via graphene hybridization. J. Adv. Ceram. 1, 72–78.

Aslam, I., Cao, C., Tanveer, M., Farooq, M.H., Khan, W.S., Tahir, M., Idrees, F., Khalid, S., 2015. A novel Z-scheme WO3/CdWO4photocatalyst withenhanced visible-light photocatalytic activity forthe degradation of organic pollutants. RSCAdv. 5, 6019–6026.

Dirany, N., Hallaoui, A., Valmalette, J.C., Arab, M., 2020. Effect of morphology and temperature treatment control on the photocatalytic and photoluminescence properties of SrWO₄ crystals. Photochem. Photobiol. Sci. 19, 235–250.

Pourmortazavi, S.M., Nasrabadi, M.R., Reza Ganjali, M., Karimi, M.S., Norouzi, P., Faridbod, F., 2017. Facile and effective synthesis of praseodymium tungstate nanoparticles through an optimized procedure and investigation of photocatalytic activity. Open Chem. 15 (1), 129–138.

Saravanakumar, S., Sivaganesh, D., Sasikumar, S., Arunpandian, M., Archana, R., 2019. Structural and photocatalytic analysis of NiWO₄ materials. Int. J. Eng. Adv. Technol. 9 (1S4), 347–351.

Botsa, S.M., Basavaiah, K., 2020. Fabrication of multifunctional TANI/Cu₂O/Ag nanocomposite for environmental abatement. Sci. Rep. 10, 14080.